

Machine learning prediction errors better than DFT accuracy

Felix A. Faber,^{1,2} Luke Hutchison,^{3,2} Bing Huang,¹ Justin Gilmer,³ Samuel S. Schoenholz,³ George E. Dahl,³ Oriol Vinyals,⁴ Steven Kearnes,³ Patrick F. Riley,³ and O. Anatole von Lilienfeld^{1,*}

¹*Institute of Physical Chemistry and National Center for Computational Design and Discovery of Novel Materials, Department of Chemistry, University of Basel, Klingelbergstrasse 80, CH-4056 Basel, Switzerland*

²*Authors contributed equally*

³*Google, 1600 Amphitheatre Parkway, Mountain View, CA, US - 94043 CA*

⁴*Google, 5 New Street Square, London EC4A 3TW, UK*

(Dated: February 5, 2022)

We investigate the impact of choosing regressors and molecular representations for the construction of fast machine learning (ML) models of thirteen electronic ground-state properties of organic molecules. The performance of each regressor/representation/property combination is assessed using learning curves which report out-of-sample errors as a function of training set size with up to $\sim 117k$ distinct molecules. Molecular structures and properties at hybrid density functional theory (DFT) level of theory used for training and testing come from the QM9 database [Ramakrishnan et al, *Scientific Data* **1** 140022 (2014)] and include dipole moment, polarizability, HOMO/LUMO energies and gap, electronic spatial extent, zero point vibrational energy, enthalpies and free energies of atomization, heat capacity and the highest fundamental vibrational frequency. Various representations from the literature have been studied (Coulomb matrix, bag of bonds, BAML and ECFP4, molecular graphs (MG)), as well as newly developed distribution based variants including histograms of distances (HD), and angles (HDA/MARAD), and dihedrals (HDAD). Regressors include linear models (Bayesian ridge regression (BR) and linear regression with elastic net regularization (EN)), random forest (RF), kernel ridge regression (KRR) and two types of neural networks, graph convolutions (GC) and gated graph networks (GG). Out-of sample errors are strongly dependent on the choice of representation *and* regressor *and* molecular property. Electronic properties are typically best accounted for by MG and GC, while energetic properties are better described by HDAD and KRR. The specific combinations with the lowest out-of-sample errors in the $\sim 117k$ training set size limit are dipole moment (MG/GC), static polarizability (MG/GG), HOMO/LUMO eigenvalue and gap (MG/GC), electronic spatial extent (BOB/KRR), zero point vibrational energy (HDAD/KRR), (free) energies and enthalpies of atomization (HDAD/KRR), heat capacity at room temperature (HDAD/KRR), and highest fundamental vibrational frequency (BAML/RF). We present numerical evidence that ML model predictions deviate from DFT less than DFT deviates from experiment for all properties. Furthermore, our out-of-sample prediction errors with respect to hybrid DFT reference are on par with, or close to, chemical accuracy. Our findings suggest that ML models could be more accurate than hybrid DFT if explicitly electron correlated quantum (or experimental) data was available.

I. INTRODUCTION

Due to its favorable trade-off between accuracy and computational cost, Density Functional Theory (DFT)^{1,2} is the work-horse of quantum chemistry³—despite its well known shortcomings regarding spin-states, van der Waals interactions, and chemical reactions^{4,5}. Failures to predict reaction profiles are particularly worrisome⁶, and recent analysis casts even more doubts on the usefulness of DFT functionals obtained through parameter fitting⁷. The prospect of universal and computationally much more efficient machine learning (ML) models, trained on data from experiments or generated at higher levels of electronic structure theory such as post-Hartree Fock or quantum Monte Carlo (e.g. exemplified in Ref.⁸), therefore represents an appealing alternative to DFT. Not surprisingly, a lot of recent effort has been devoted to developing ever more accurate ML models of properties of molecular and condensed phase systems.

Several ML studies have already been published using a data set called QM9⁹, consisting of molecular quantum

properties for the $\sim 134k$ smallest organic molecules containing up to 9 heavy atoms (C, O, N, or F; not counting H) in the GDB-17 universe¹⁰. Some of these studies have developed or used representations we consider in this work, such as BAML (Bonds, angles, machine learning)¹¹, bag of bonds (BoB)^{12,13} and the Coulomb matrix (CM)^{13,14}. Atomic variants of the CM have also been proposed and tested on QM9¹⁵. Other representations have also been benchmarked on QM9 (or QM7 which is a smaller but similar data set), such as Fourier series of radial distance distributions¹⁶, motifs¹⁷, the smooth overlap of atomic positions (SOAP)¹⁸ in combination with regularized entropy match¹⁹, constant size descriptors based on connectivity and encoded distance distributions²⁰. Ramakrishnan *et al.*⁸ introduced a Δ -ML approach, where the difference between properties calculated at coarse/accurate quantum level of theories is being modeled. Furthermore, neural network models, as well as deep tensor neural networks, have recently been proposed and tested on the same or similar data sets^{21,22}. Dral *et al.*²³ use such data to machine learn

optimal molecule specific parameters for the OM2²⁴ semi-empirical method, and orthogonalization tests are benchmarked in Ref.²⁵.

However, limited work has yet been done in systematically assessing *various* methods *and* properties on large sets of the exact same chemicals²⁶. In order to unequivocally establish if ML has the potential to replace DFT for the screening of properties, one has to demonstrate that ML test errors are systematically lower than estimated DFT accuracies for all the properties available. This study accomplishes that through a large scale assessment of unprecedented scale: (i) In order to approximate large training set sizes N , we included 13 quantum properties from up to $\sim 117\text{k}$ molecules in training (90% of QM9). (ii) We tested multiple regressors (Bayesian ridge regression (BR), linear regression with elastic net regularization (EN), random forest (RF), kernel ridge regression (KRR), neural network (NN) models graph convolutions (GC)²⁷ and gated graphs (GG)²⁸) and (iii) multiple representations including BAML, BOB, CM, extended connectivity fingerprints (ECFP4), histograms of distance, angle, and dihedral (HDAD), molecular alchemical radial angular distribution (MARAD), and molecular graphs (MG). (iv) We investigated *all* combinations of regressors and representations, except for MG/NN which was exclusively used together because GC and GG depend fundamentally on the input representation being a graph instead of a flat feature vector.

The best models for the various properties are: dipole moment (MG/GC), static polarizability (MG/GG), HOMO/LUMO eigenvalue and gap (MG/GC), electronic spatial extent (BOB/KRR), zero point vibrational energy (HDAD/KRR), atomization energy at 0 Kelvin (HDAD/KRR), atomization energy at room temperature (HDAD/KRR), enthalpy of atomization at room temperature (HDAD/KRR), atomization of free energy at room temperature (HDAD/KRR), heat capacity at room temperature (HDAD/KRR), and the highest fundamental vibrational frequency (BAML/RF). For training set size of $\sim 117\text{k}$ (90% of data set) we have found the additional out-of-sample error added by machine learning to be lower or as good as DFT errors relative to experiment for all properties, and that chemical accuracy (See table III) is reached, or in sight.

This paper is organized as follows: First we will briefly describe the methods, including data set, model validation protocols, representations, and regressors. In section III, we present the results and discuss them, and section IV concludes the paper.

II. METHOD

A. Data set

We have used the QM9 data set consisting of $\sim 134\text{k}$ drug-like organic molecules⁹. Molecules in the data set consist of H, C, O, N and F, and contain up to 9

heavy atoms. For each molecule several properties, calculated at DFT level of theory (B3LYP/6-31G(2df,p)), were included. We used: Norm of dipole moment μ (Debye), norm of static polarizability α (Bohr³), HOMO eigenvalue $\varepsilon_{\text{HOMO}}$ (eV), LUMO eigenvalue $\varepsilon_{\text{LUMO}}$ (eV), HOMO-LUMO gap $\Delta\varepsilon$ (eV), electronic spatial extent $\langle R^2 \rangle$ (Bohr²), zero point vibrational energy ZPVE (eV), atomization energy at 0 Kelvin U_0 (eV), atomization energy at room temperature U (eV), enthalpy of atomization at room temperature H (eV), atomization of free energy at room temperature G (eV), heat capacity at room temperature C_v (cal/mol/K), and the highest fundamental vibrational frequency ω_1 (cm⁻¹). For energies of atomization (U_0 , U , H and G) all models yield very similar errors: We will only discuss for U_0 for the remainder. The 3053 molecules specified in Ref.⁹ which failed SMILES consistency tests were excluded from our study, as well as two linear molecules, leaving $\sim 131\text{k}$ molecules.

B. Model validation

Starting from the $\sim 131\text{k}$ molecules in QM9 after removing the $\sim 3\text{k}$ molecules (see above) we have created a number of train-validation-test splits. We have split the data set into test and non-test sets and varied the percentage of data in test set to explore the effect of amount of data in error rates. Inside the non-test set, we have performed 10 fold cross validation for hyperparameter optimization. That is, for each model 90% (the training set) of the non-test set is used for training and 10% (the validation set) is used for hyperparameter selection. For each test/non-test split, we have trained 10 models on different subsets of the non-test set, and we report the mean error on the test set across those 10 models. Note that the non-test set will be referred to as training set in the results section in order to simplify discussion.

In terms of CPU investments necessary for training the respective models we note that EN/BR, RF/KRR, and GC/GG required minutes, hours, and multiple days, respectively. Using GPUs could dramatically reduce such timings.

C. DFT errors

To place the quality of our prediction errors in the right context, experimental accuracy estimates of DFT become desirable. Here, we summarize literature results comparing DFT to experiments for the various properties we study. Where data is available, the corresponding deviation of DFT from experiment is listed in Table III, alongside our ML prediction errors (*vide infra*). More specifically, rough hybrid DFT error estimates for dipole moment and polarizability have been obtained from Refs.^{4,29}.

Frontier molecular orbital energies (HOMO, LUMO and HOMO-LUMO gap) can not be measured directly. However, for the exact (yet unknown) exchange-correlation potential, HOMO and LUMO eigenvalues correspond to the negative of the vertical ionization potential (IP) and electron affinity (EA), respectively³⁰. In order to quantify the accuracy of DFT (B3LYP/6-31G(2df,p)) based frontier eigenvalues, we have carried out additional corresponding calculations for a set of 28 organic molecules with up to 9 heavy atoms (not counting hydrogen) for which experimental (adiabatic) IPs and EAs were reported for NIST³¹, or in Ref.³² (see also Table S2 in supplementary materials). Ignoring the (possibly severe) difference between vertical and adiabatic values, we thus approximate DFT errors of HOMO/LUMO energies by their respective deviation from experimentally measured IPs and EAs. Correspondingly, we estimate the HOMO-LUMO gap error by comparison to the experimental IP/EA gap.

DFT RMSE estimates of ZPVE and ω_1 (the highest fundamental vibrational frequency) were published in Ref.³³ for a set of 41 organic molecules, with up to 6 heavy atoms (not counting hydrogen) and calculated using B3LYP/cc-pVTZ (assuming a normal distribution, we have calculated corresponding MAEs using a scaling factor of ~ 0.8 ³⁴). DFT errors estimates of energies of atomization have been taken from Ref.³⁵. The errors were estimated from 69 organic molecules (22 hydrocarbons and 47 substituted hydrocarbons), with up to 6 heavy atoms (not counting hydrogens), and calculated using B3LYP/6-311+G(3df,2p). Deviation of DFT (at the B3LYP/6-311g** level of theory) from experimental heat capacities were reported by DeTar³⁶ who obtained errors of 16 organic molecules, with up to 8 heavy atoms (not counting hydrogens). No satisfactory experimental data for electronic spacial extent has been found in the literature.

Note, however, that one should be cautious when referring to these errors: Strictly speaking they can not be compared since different basis sets, molecules, and experiments were used. Nevertheless, we feel that the quoted errors provide meaningful guidance as to what one can expect from DFT for each property.

D. Representations

1. CM and BoB

The Coulomb matrix (CM) representation¹⁴ is a square atom by atom matrix, where off diagonal elements are the Coulomb nuclear repulsion terms between atom pairs. The diagonal elements approximate the electronic potential energy of the free atoms. Atom indices in the CM are sorted by the L^1 norm of each atom’s row (or column). The Bag of Bonds (BoB)¹² representation uses exclusively CM elements, grouping them for different atom pairs into different bags, and sorting them within each

bag by their relative magnitude.

2. BAML

The recently introduced BAML (Bonds, angles, machine learning) representation can be viewed as a many-body extension of BoB¹¹. All pairwise nuclear repulsions are replaced by Morse/Lennard-Jones potentials for bonded/non-bonded atoms respectively. Furthermore, three- and four-body interactions between covalently bonded atoms are included using angular and torsional terms, respectively. Parameters and functional forms are based on the universal force field (UFF)³⁷.

3. ECFP4

Extended Connectivity Fingerprints³⁸ (ECFP4) are a common representation of molecules in cheminformatics based studies. They are particularly popular for drug discovery^{39–41}. The basic idea, typical also for other cheminformatics descriptors⁴² (e.g. the *signature* descriptor^{43,44}) is to represent a molecule as the set of subgraphs up to a fixed diameter (here we use ECFP4, which is a max diameter of 4 bonds). To produce a fixed length vector, the subgraphs can be hashed such that every subgraph sets one bit in the fixed length vector to 1. In this work, we use a fixed length vector of size 1024. Note that ECFP4 is based solely on the molecular graph specifying all covalent bonds, e.g. as encoded by SMILES strings.

4. MARAD

Molecular atomic radial angular distribution (MARAD) is a radial distribution function (RDF) based representation. MARAD is an extension of an atomic representation ARAD, consisting of three RDFs for distances between atom pairs, and parallel and orthogonal projections of distances in atom triplets, respectively. Distances between two molecules can be evaluated analytically. Unfortunately, most regressors evaluated in this work, such as BR, EN and RF, do not rely on inner products and distances between representations. We remedy this issue by projecting MARAD onto bins in order to work with all regressors (apart for GG and GC which use MG exclusively). Further technical details regarding MARAD are specified in the Supplementary materials⁴⁵.

5. HD, HDA, and HDAD

BOB, BAML and MARAD rely on computing functions for given interatomic distances, and/or angles, and/or torsions, and then either project that value onto

discrete bins, or sort the values. As a straightforward alternative, we also investigated representations which account directly from pairwise distances, triple-wise angles, and quad-wise dihedral angles through manually generated bins in histograms. The resulting representations in increasing interatomic many-body order are called HD (Histogram of distances), HDA (Histogram of distances and angles), and HDAD (Histogram of distances, angles and dihedral angles). For any given molecule, one iterates through each atom a_i , producing a set of distances, angle and dihedral angle features for a_i .

Distance features were produced by measuring the distance between a_i and a_j (for $i \neq j$) for each element pair. The distance features were assigned a label incorporating the atomic symbols of a_i and a_j sorted alphabetically (with H last), e.g. if a_i was a carbon atom and a_j was a nitrogen atom, the distance feature for the atom pair would be labeled C-N. These labels will be used to group all features with the same label into a histogram and allow us to only count each pair of atoms once.

Angle features were produced by taking the principal angles formed by the two vectors spanning from each atom a_i to every subset of 2 of its 3 nearest atoms, a_j and a_k . The angle features were labeled by the element type of a_i , followed by the alphabetically sorted element types (Except for hydrogens, which were listed last) of a_j and a_k . The example where a_i is a Carbon atom, a_j a Hydrogen atom, a_k a Nitrogen would be assigned the label C-N-H.

Dihedral angle features were produced by taking the principal angles between two planes. We take a_i as the origin, and for each of the four nearest neighbors in turn, labeling the neighbor atom a_j , and forming a vector $V_{ij} = a_i \rightarrow a_j$. Then all $\binom{3}{2}$ subsets of the remaining three out of four nearest neighbors of a_i are chosen, and labeled as a_k and a_l . This third and fourth atom respectively form two triangular faces when paired with V_{ij} : $\langle a_k, a_i, a_j \rangle$ and $\langle a_l, a_i, a_j \rangle$. The dihedral angle between the two triangular faces was calculated. These dihedral angle features were labeled with the atomic symbol for a_i , followed by the atomic symbols for a_j , a_k and a_l , sorted alphabetically, with the exception that hydrogens were listed last, e.g. C-C-N-H.

The features from all molecules have been aggregated for each label type to generate a histograms for each label type. Fig. 1 exemplifies this for C-N distances, C-C-C angles, and C-C-C-O dihedrals for the entire QM9 data set. Certain typical molecular characteristics can be recognized upon mere inspection. For example, the CN histogram displays a strong and isolated peak between 1.1 and 1.5 Å, corresponding to occurrences of single, double, and triple bonds. For distances above 2 Å, peaks at typical radii of second and third covalent bonding shells around N can be recognized at 2.6 Å and 3.9 Å. Also C-C-C angles can be easily interpreted: The peak close to zero and π Rad corresponds to geometries where three atoms are part of a linear (alkyne, or nitrile) type of motif. The broad and largest peak corresponds to 120 and

109 degrees, typically observed in sp^2 and sp^3 hybridized atoms.

The morphology of each histogram has then been examined to identify apparent peaks and troughs, motivated by the idea that peaks indicate structural commonalities among molecules. Bin centers have been placed at each significant local minimum and maximum (Shown as vertical lines in Fig. 1). Values at 15-25 bin centers have been chosen as a representation for each label type. All bin center values are provided in the Supplementary Material. For each molecule, the collection of features has subsequently been rendered into a fixed-size representation, producing one vector component for each bin center, within each label type. This has been accomplished following a two-step process. (i) *Binning and interpolation*: Each feature value is projected on the two nearest bins. The relative amount projected on each bin uses linear projection between the two bins. For example: A feature with value 1.7 which lies between two bins placed at 1.0 and 2.0 respectively, contributes 0.3 and 0.7 to the first and second bin respectively. (ii) *Reduction*: The collection of contributions within each bin of each molecule’s feature vector is condensed to a single value by summing all contributions.

6. Molecular Graphs

We have investigated several neural network models which are based on molecular graphs (MG) as representation. The inputs are real-valued vectors associated with each atom and with each pair of atoms. More specifically, we have used the featurization described in Kearnes *et al.*²⁷ with the removal of partial charge and the addition of Euclidean distances to the pair feature vectors. All elements of the feature vector are described in Tables I and II.

The featurization process was unsuccessful for a small number of molecules (367) because of conversion failures from geometry to rational SMILES string when using OpenBabel⁴⁶ or RDKit⁴⁷, and were excluded from all results using the molecule graph features.

TABLE I. Atom features for the MG representation: Values provided for each atom in the molecule.

Feature	Description
Atom type	H, C, N, O, F (one-hot).
Chirality	R or S (one-hot or null).
Formal charge	Integer electronic charge.
Ring sizes	For each ring size (3–8), the number of rings that include this atom.
Hybridization	sp , sp^2 , or sp^3 (one-hot or null).
Hydrogen bonding	Whether this atom is a hydrogen bond donor and/or acceptor (binary values).
Aromaticity	Whether this atom is part of an aromatic system.

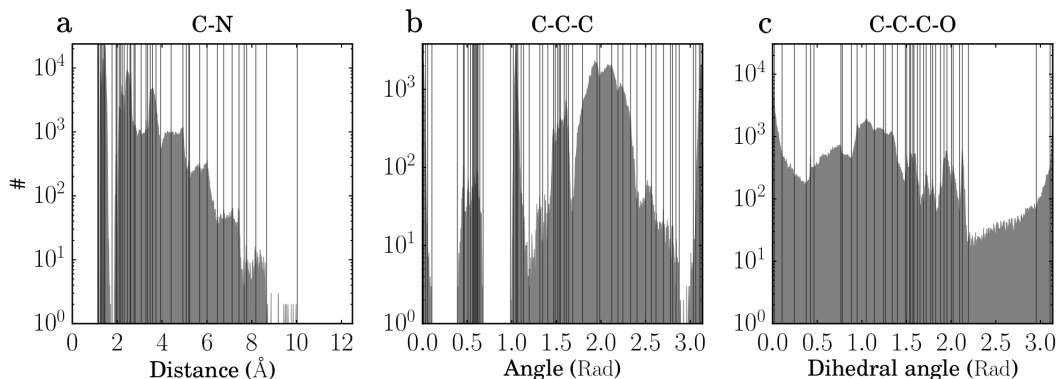


FIG. 1. Illustration of select histograms of distances, angles and dihedral angles in QM9. Vertical lines constitutes placements of the bins in the HD and/or HDAD representations. (a) All C-N distances. (b) All C-C-C angles. (c) All C-C-C-O dihedral angles.

TABLE II. Atom pair features for the MG representation: Values provided for each pair of atoms in the molecule.

Feature	Description
Bond type	Single, double, triple, or aromatic (one-hot or null).
Graph distance	For each distance (1–7), whether the shortest path between the atoms in the pair is less than or equal to that number of bonds (binary values).
Same ring	Whether the atoms in the pair are in the same ring.
Spatial distance	The euclidean distance between the two atoms.

Note that within a previous draft of this study⁴⁸, we reported biased results for GC/GG models due to use of Mulliken partial charges within the MG representation. All MG results presented herewithin have been obtained without any Mulliken charges in the representation. Model hyper parameters for the GC model, however, still correspond to the previously obtained hyper parameter search.

E. Regressors

For all methods, we first standardized the property values so that all properties have zero mean and unit standard deviation.

1. Kernel Ridge Regression

KRR^{49–52} is a type of regression with regularization⁵³ which uses kernel functions as basis set. A property p of a query molecule \mathbf{m} is predicted by a sum of weighted kernel functions $K(\mathbf{m}, \mathbf{m}_i^{\text{train}})$ between \mathbf{m} and all molecules $\mathbf{m}_i^{\text{train}}$ in the training set,

$$p(\mathbf{m}) = \sum_i^N \alpha_i K(\mathbf{m}, \mathbf{m}_i^{\text{train}}) \quad (1)$$

where α_i are regression coefficients, obtained by minimizing the Euclidean distance between the estimated and the reference property of all molecules in the training set. We used Laplacian and Gaussian kernels as implemented by scikit-learn⁵⁴ for all representations.

The level of noise in our data is very low so strong regularization is not necessary. We therefore set the regularization parameter to 10^{-9} . Kernel widths were chosen by screening values on a base-2 logarithmic grid for the 10 percent training set (from 0.25 to 8192 for Gaussian kernel and 0.1 to 16384 for Laplacian kernel). In order to simplify the width screening, prior to learning all feature vectors were normalized (scaling the input vector by the mean norm across the training set) by the Euclidean norm for the Gaussian kernel and the Manhattan norm for the Laplacian kernel.

2. Bayesian Ridge Regression

We use BR⁵⁵ as is implemented in scikit-learn⁵⁴. BR is a linear model with a L^2 penalty on the coefficients. Unlike Ridge Regression where the strength of that penalty is a regularizing hyperparameter which must be set, in Bayesian Ridge Regression the optimal regularizer is estimated from the data.

3. Elastic Net

Also EN⁵⁶ is a linear model. Unlike BR, the penalty on the weights is a mix of L^1 and L^2 terms. In addition to the regularizing hyperparameter for the weight penalty, Elastic net has an additional hyperparameter `l1_ratio` to

control the relative strength of the L^1 and L^2 weight penalties. We used the scikit-learn⁵⁴ implementation and set `l1_ratio` = 0.5. We then did a hyperparameter search on regularizing parameter in a base 10 logarithmic grid from $1e-6$ to 1.0.

4. Random Forest

We use RF⁵⁷ as implemented in scikit-learn⁵⁴. RF regressors produce a value by averaging many individual decision trees fitted on randomly resampled sets of the training data. Each node in each decision tree is a threshold of one input feature. Early experiments did not reveal strong differences in performance based on the number of trees used, once a minimal number was reached. We have used 120 trees for all regressions.

5. Graph Convolutions

We have used the GC model as described in Kearnes *et al.*²⁷, with several structural modifications and optimized hyperparameters. The graph convolution model is built on the concepts of “atom” layers (one real vector associated with each atom) and “pair” layers (one real vector associated with each pair of atoms). The graph convolution architecture defines operations to transform atom and pair layers to new atom and pair layers. There are three structural changes to the model used herewithin when compared to the one described in Kearnes *et al.*²⁷. We describe these briefly here with details in the Supplementary Material. First, we have removed the “Pair order invariance” property by simplifying the $(A \rightarrow P)$ transformation. Since the model only uses the atom layer for the molecule level features, pair order invariance is not needed. Second, we have used the Euclidean distance between atoms. In the $(P \rightarrow A)$ transformation, we divide the value from the convolution step by a series of distance exponentials. If the original convolution for an atom pair (a, b) with distance d produces a vector V , we concatenate the vectors V , $\frac{V}{d^1}$, $\frac{V}{d^2}$, $\frac{V}{d^3}$, and $\frac{V}{d^6}$ to produce the transformed value for the pair (a, b) . Third, we have followed other work on neural networks based on chemical graphs⁵⁸. Inspired by fingerprinting like Extended Connectivity Fingerprints³⁸, based on summing softmax operations to convert a real valued vector to a sparse vector and sum those sparse vectors across all the atoms, we have used the same operation here along with a simple sum across the atoms to produce molecule level features from the top atom layer. We have found that this works as well or better than the Gaussian histograms first used in GC²⁷. To optimize the network, we have searched the hyperparameter space using Gaussian Process Bandit Optimization⁵⁹ as implemented by HyperTune⁶⁰. The hyperparameter search has been based on the evaluation of the validation set for a single fold of the data. Further details including parameters, and

search ranges chosen for this paper are listed in the Supplementary materials⁴⁵.

6. Gated Graph Neural Networks

We have used the GG Neural Networks model (GG) as described in Li *et al.*²⁸. Similar to the GC model, it is a deep neural network whose input is a set of node features $\{x_v, v \in G\}$, and an adjacency matrix A with entries in a discrete set $S = \{0, 1, \dots, k\}$ to indicate different edge types. It has internal hidden representations for each node in the graph h_v^t of dimension d which it updates for T steps of computation. Its output is invariant to all graph isomorphisms, meaning the order of the nodes presented to the model does not matter. We have implemented the GG model as described in the original work with some additional preprocessing of the input. To include distance information we bin atomic distances into 10 bins, $[0, 2]$, $[2, 2.5]$, $[2.5, 3]$, $[3, 3.5]$, $[3.5, 4]$, $[4, 4.5]$, $[4.5, 5]$, $[5, 5.5]$, $[5.5, 6]$, and $[6, \infty]$ in Å, respectively. Using these bins, the adjacency matrix has entries in an alphabet of size 14 ($k=14$), indicating bond type for covalently bonded atoms, and distance bin for all other atoms. We have trained the GG model on each target property individually. Further technical details are specified in the Supplementary materials⁴⁵.

III. RESULTS AND DISCUSSION

A. Overview

We present an overview of the most relevant numerical results in Table III. It contains the test errors for all combinations of regressors and representations and properties for models trained on ~ 117 k molecules. The best models for the respective properties are μ (MG/GC), α (MG/GG), ϵ_{HOMO} (MG/GC), ϵ_{LUMO} (MG/GC), $\Delta\epsilon$ (MG/GC), $\langle R^2 \rangle$ (BOB/KRR), ZPVE (HDAD/KRR), U_0 (HDAD/KRR), C_v (HDAD/KRR), and ω_1 (BAML/RF). We do not show results for the other three energies, $U(T = 298K)$, $H(T = 298K)$, $G(T = 298K)$ since identical observations as for U_0 can be made.

Overall, NN and KRR regressors perform well for most properties. The ML out-of-sample errors outperform DFT accuracy and reach chemical (target) accuracy, both defined alongside in table III, for μ (GC), $\langle R^2 \rangle$ (BOB/KRR), U_0 (HDAD/KRR and MG/GG), C_v (HDAD/KRR), and ω_1 (BAML/KRR, MG/GC, HDAD/KRR, BOB/KRR, HD/KRR and MG/GG). For the remaining properties (α , ϵ_{HOMO} , ϵ_{LUMO} , $\Delta\epsilon$, and ZPVE) the best models come within a factor 2 of target accuracy, while all outperforming hybrid DFT accuracy.

In Fig. 2 out-of-sample errors as a function of training set size (learning curves) are shown for all properties and representations with the best corresponding regressor. It

is important to note that *all* models on display systematically improve with training set size, exhibiting the typical linearly decaying behavior on a log-log plot^{11,62}. Errors for most models shown decay with roughly the same slopes, indicating similar exponents in the power-law of error decay. Notable exceptions, i.e. property models with considerably steeper learning curves, are MG/GC for μ , MG/GG and HDAD/KRR for α , CM/KRR and BoB/KRR for $\langle R^2 \rangle$, HDAD/KRR and MG/GG for U_0 , and MG/GG for ω_1 . These results suggest that the specified representations capture particularly well the effective dimensionality of the corresponding property in chemical space.

B. Regressors

Inspection of Table III indicates that the regressors can roughly be ordered by performance, independent of property and representation: GC>GG>KRR>RF>BR>EN. It is noteworthy how EN, BR, and RF regressors perform substantially worse than GC/GG/KRR. This can also be seen from the learning curves of all regressors presented in Figures S1 to S6 of the Supplementary Material. The performance of BR and EN improves only slightly with increased training set size and even gets worse for some property/representation combinations. These two regressors also exhibit very similar learning curves and BR preforms only slightly better than EN for most combinations. The only clear exception to this rule is for ZPVE and U_0 together with HDAD, where BR preforms significantly better than EN. Also, BR and EN errors rapidly converge to a constant w.r.t. training set size for all representations and properties, except for HDAD, which is the only representation which has a noteworthy improvement with increased training set size for some properties. The constant learning rates are not surprising as (a) the number of free regression parameters in BR and EN is relatively small and does not grow with training set size, and as (b) the underlying model is a linear combination with small flexibility. This behavior implies error convergence already for relatively small training sets.

RF performs poorly compared to GC, GG and KRR for all properties except for ω_1 , the highest lying fundamental vibrational frequency in each molecule. For this property RF yields an astounding performance with out-of-sample errors as small as single digit cm^{-1} . B3LYP achieves a mean absolute error of only 28 cm^{-1} with respect to experiment³³. The distribution of ω_1 , Figure 1 of reference¹³, suggests a simple reason for this: There are three distinct peaks which correspond to typical C-H, N-H and O-H stretch vibrations in increasing order. Therefore the principal learning task in this property is to detect if there is an OH group, and if not if there is an NH group. If neither group is present, CH will yield the vibration with the highest frequency. As such, this is essentially about classifying which bonds are present in

the molecule. RF works by fitting a decision tree to the target property. Each branch in the tree is based on an inequality of *one* entry in the representation. RF should therefore be able to identify which bonds are present in a molecule, simply by looking at the entries in the each element pair, and/or triplet bin of the representations. For RF, a fractional importance can be assigned to each input feature (the sum of all importances is 1.0). Analyzing the importance of the bins in HDAD of the RF model reveals that the three bins with highest importance are: O-H placed at 0.961 \AA , N-H placed at 1.01 \AA and C-C-H at 3.138 radians with an importance of 0.587 , 0.305 and 0.064 respectively. These three first bins constitute $\sim 96\%$ of the prediction of ω_1 and distances of the O-H and N-H bins are very similar to O-H and N-H bond lengths. C-C-H is placed on $\sim \pi$ radians which means that it has to correspond to a linear C-C-H (alkyne) chain which implies that the two carbons must be bonded by a triple bond (typically the C-H with the lowest pK_a and the highest C-H stretch vibration).

KRR performs remarkably well on average. For energetic properties, as well as $\langle R^2 \rangle$, it yields the lowest overall errors in combination with HDAD and BoB, respectively. Its outstanding performance is not unsurprising in light of the multiple previous ML studies dealing with compositional as well as configurational spaces. The neural network flavors GC and GG, however, yield better performance on average, and the lowest errors for all electronic properties, i.e. dipolemoment, polarizability, HOMO/LUMO eigenvalues and gaps.

C. Representations

As one would expect, HDAD contains more relevant information and thus it always outperforms HD when using KRR. Tests also showed that an HDA representation systematically yields errors in between HDAD and HD, and similar observations hold for BR and EN regressor. In the case of RF, however, we observe little difference between HDAD and HD, and HD can even yield slightly lower errors than HDAD. In our opinion, this is due to the additional bins of angles and dihedrals rather adding noise than signal. By contrast, the separation of distances, angles and dihedral angles into different bins is not a problem for the KRR methods because the kernels used are purely distance based. This makes it possible for KRR to exploit the extra three- and four-body information in HDAD and to gain an advantage over HD. We note however that the remarkable performance of HDAD is possible despite its striking simplicity. As illustrated in Fig. 1 and discussed above, characteristic chemical behavior can be directly obtained by human inspection of HDAD. As such, HDAD corresponds to a representation very much "Occam's razor style". Unfortunately, due to its discrete nature and its origin in sorting distances, HDAD will suffer from lack of differentiability, which might limit its applicability when modeling forces

or other non-equilibrium properties.

MARAD, in principle containing the same information as HDA, performs similarly to BAML—yet, MARAD requires no prior knowledge about the physics encoded in the universal force-field. BoB and CM, while previously considered state of the art, result in relatively poor performance except for $\langle R^2 \rangle$ where BoB/KRR gives the lowest overall error. The simple bag of bonds, representing lists of all the pairwise Coulombic interactions appears to coincide ideally with the corresponding electronic spread in the molecule. Due to its inherent lack of uniqueness, however, we believe that also this property must converge to a finite error in the limit of infinite training set size. ECFP4 produces out-of-sample errors on par or slightly better than CM/KRR for intensive properties (μ , HOMO/LUMO eigenvalues and gap), however the model produces errors that are off-the-chart for all extensive properties (α , $\langle R^2 \rangle$, ZPVE, U_0 and C_V).

IV. CONCLUSIONS

We have benchmarked many combinations of regressors and representations on the same QM9 data set consisting of $\sim 131k$ organic molecules. For all properties, the best ML model prediction errors reach the accuracy of hybrid DFT with respect to experiment. For 8 out of 13 distinct properties (atomization energies, heat-capacity, ω_1 , $\langle R^2 \rangle$, μ) out-of-sample errors reach levels on par with chemical accuracy, or better, using a training set size of $\sim 117k$ (90% of QM9 data set) molecules. For the remaining properties α , ϵ_{HOMO} , ϵ_{LUMO} , $\Delta\epsilon$, and ZPVE, errors of the best models come within a factor 2 of chemical accuracy.

Regressors EN, BR, and RF lead to rather high out-of-sample errors, while KRR and graph based NN regressors compete for the lowest errors. We have found that GC, GG, and KRR have best performance across *all* properties, except for the highest vibrational frequency for which RF performs best. There is no single representation and regressor combination that works best for all properties (though forthcoming work with further improvements to the GG based models indicates best in class performance across all properties⁶³). For intensive electronic properties (μ , HOMO/LUMO eigenvalues and gap) we have found MG/NN to yield the highest predictive power, while HDAD/KRR corresponds to the most accurate model for extensive properties (α , $\langle R^2 \rangle$, ZPVE, U_0 and C_V). The latter point is remarkable when considering the simplicity of KRR, being just a linear expansion of property in training set, and HDAD, being just histograms of distances, angles, dihedrals. Using BR and EN is not recommended if accuracy is of importance, both regressors perform worse across all proper-

ties. Apart from predicting highest fundamental vibrational frequency best, RF based models deliver rather unsatisfactory performance. The ECFP4 based models have shown poor general performance in comparison to all other representations studied; it is not recommended for investigations of molecular properties.

We should caution the reader that all our results refer to equilibrium structures of a set of only $\sim 131k$ organic molecules. While $\sim 131k$ molecules might seem sufficiently large to be representative, this number is dwarfed in comparison to chemical space, i.e. the space populated by all theoretically stable molecules, estimated to exceed 10^{60} for medium sized organic molecules⁶⁴. Furthermore, ML models for predicting properties of molecules in non-equilibrium or strained configurations might require substantially more training data. This point is also of relevance because some of the highly accurate models described herewithin (MG based) currently use bond based graph connectivity in addition to distance, raising questions about the applicability to reactive processes.

In summary, for the organic molecules studied, we have collected numerical evidence which suggests that the out-of-sample error of ML is consistently better than estimated DFT accuracy. While this does not prove that ML models would reach same error levels if more accurate, explicitly electron correlated or experimental reference data was used, there are studies which suggest that relevant property approximations do become smoother when using higher levels of theory^{8,65}. As such, our study indicates that future reference data sets for training modern state-of-the-art machine learning models will require levels of theory which go beyond hybrid DFT. Finally, we note that future work could deal with improving representations and regressors with the goal of reaching similar predictive power using less data.

ACKNOWLEDGMENTS

The authors thank Dirk Bakowies for helpful comments, and Adrian Roitberg for pointing out an issue with the use of partial charges in the neural net models in an earlier version of this paper. O.A.v.L. acknowledges support from the Swiss National Science foundation (No. PP00P2_138932, 310030_160067), the research fund of the University of Basel, and from Google. This material is based upon work supported by the Air Force Office of Scientific Research, Air Force Material Command, USAF under Award No. FA9550-15-1-0026. This research was partly supported by the NCCR MARVEL, funded by the Swiss National Science Foundation. Some calculations were performed at sciCORE (<http://scicore.unibas.ch/>) scientific computing core facility at University of Basel.

* anatole.vonlilienfeld@unibas.ch

¹ P. Hohenberg and W. Kohn, Phys. Rev. **136**, B864 (1964).

- ² W. Kohn and L. J. Sham, Phys. Rev. **140**, A1133 (1965).
- ³ K. Burke, J. Chem. Phys. **136**, 150901 (2012).
- ⁴ W. Koch and M. C. Holthausen, *A Chemist's Guide to Density Functional Theory* (Wiley-VCH, 2002).
- ⁵ A. J. Cohen, P. Mori-Sánchez, and W. Yang, Chem. Rev. **112**, 289 (2012).
- ⁶ R. E. Plata and D. A. Singleton, J. Am. Chem. Soc. **137**, 3811 (2015).
- ⁷ M. G. Medvedev, I. S. Bushmarinov, J. Sun, J. P. Perdew, and K. A. Lyssenko, Science **355**, 49 (2017).
- ⁸ R. Ramakrishnan, P. O. Dral, M. Rupp, and O. A. von Lilienfeld, J. Chem. Theory Comput. **11**, 2087 (2015).
- ⁹ R. Ramakrishnan, P. O. Dral, M. Rupp, and O. A. von Lilienfeld, Sci. Data **1** (2014).
- ¹⁰ L. Ruddigkeit, R. van Deursen, L. C. Blum, and J.-L. Reymond, J. Chem. Inf. Model. **52**, 2864 (2012).
- ¹¹ B. Huang and O. A. von Lilienfeld, J. Chem. Phys. **145**, 161102 (2016).
- ¹² K. Hansen, F. Biegler, R. Ramakrishnan, W. Pronobis, O. A. von Lilienfeld, K.-R. Müller, and A. Tkatchenko, J. Phys. Chem. Lett. **6**, 2326 (2015).
- ¹³ R. Ramakrishnan and O. A. von Lilienfeld, chimia **69**, 182 (2015).
- ¹⁴ M. Rupp, K.-R. Tkatchenko, Alexandre haand Müller, and O. A. von Lilienfeld, Phys. Rev. Lett. **108**, 058301 (2012).
- ¹⁵ J. Barker, J. Bulin, J. Hamaekers, and S. Mathias, arXiv preprint arXiv:1611.05126 (2016).
- ¹⁶ O. A. von Lilienfeld, R. Ramakrishnan, M. Rupp, and A. Knoll, Int. J. Quantum **115**, 1084 (2015).
- ¹⁷ T. D. Huan, A. Mannodi-Kanakkithodi, and R. Ramprasad, Phys. Rev. B **92**, 014106 (2015).
- ¹⁸ A. P. Bartók, R. Kondor, and G. Csányi, Phys. Rev. B **87**, 184115 (2013).
- ¹⁹ S. De, A. P. Bartók, G. Csányi, and M. Ceriotti, Phys. Chem. Chem. Phys. **18**, 13754 (2016).
- ²⁰ C. R. Collins, G. J. Gordon, O. A. von Lilienfeld, and D. J. Yaron, <https://arxiv.org/abs/1701.06649> (2016).
- ²¹ J. S. Smith, O. Isayev, and A. E. Roitberg, Chem. Sci. , (2017).
- ²² K. T. Schütt, F. Arbabzadah, S. Chmiela, K. R. Müller, and A. Tkatchenko, Nat. Commun. **8**, 13890 (2017).
- ²³ P. O. Dral, O. A. von Lilienfeld, and W. Thiel, J. Chem. Theory **11**, 2120 (2015).
- ²⁴ W. Weber and W. Thiel, Theor. Chem. Acc. **103**, 495 (2000).
- ²⁵ P. O. Dral, X. Wu, L. Spörkel, A. Koslowski, and W. Thiel, J. Chem. Theory **12**, 1097 (2016).
- ²⁶ K. Hansen, G. Montavon, F. Biegler, S. Fazli, M. Rupp, M. Scheffler, O. A. von Lilienfeld, A. Tkatchenko, and K.-R. Müller, J. Chem. Theory Comput. **9**, 3404 (2013).
- ²⁷ S. Kearnes, K. McCloskey, M. Berndl, V. Pande, and P. Riley, J. Comput. Aided Mol. Des. **30**, 595 (2016).
- ²⁸ Y. Li, D. Tarlow, M. Brockschmidt, and R. Zemel, ICLR (2016).
- ²⁹ A. L. Hickey and C. N. Rowley, J. Phys. Chem. A **118**, 3678 (2014).
- ³⁰ R. Stowasser and R. Hoffmann, J. Am. Chem. Soc. **121**, 3414 (1999).
- ³¹ NIST computational chemistry comparison and benchmark database, Editor: Russell D. Johnson III, <http://cccbdb.nist.gov/> (2016).
- ³² R. G. Parr and W. Yang, *Density functional theory of atoms and molecules* (Oxford Science Publications, 1989).
- ³³ P. Sinha, S. E. Boesch, C. Gu, R. A. Wheeler, and A. K. Wilson, J. Phys. Chem. A **108**, 9213 (2004).
- ³⁴ R. C. Geary, Biometrika **27**, 310 (1935).
- ³⁵ L. A. Curtiss, K. Raghavachari, P. C. Redfern, and J. A. Pople, J. Chem. Phys. **106**, 1063 (1997).
- ³⁶ D. F. DeTar, J. Phys. Chem. A **111**, 4464 (2007).
- ³⁷ A. K. Rappe, C. J. Casewit, K. S. Colwell, W. A. G. III, and W. M. Skiff, J. Am. Chem. Soc. **114**, 10024 (1992).
- ³⁸ D. Rogers and M. Hahn, J. Chem. Inf. Model. **50**, 742 (2010).
- ³⁹ J. Besnard, G. F. Ruda, V. Setola, K. Abecassis, R. M. Rodriguiz, X.-P. Huang, S. Norval, M. F. Sassano, A. I. Shin, L. A. Webster, *et al.*, Nature **492**, 215 (2012).
- ⁴⁰ E. Lounkine, M. J. Keiser, S. Whitebread, D. Mikhailov, J. Hamon, J. L. Jenkins, P. Lavan, E. Weber, A. K. Doak, S. Côté, *et al.*, Nature **486**, 361 (2012).
- ⁴¹ R. W. Huigens III, K. C. Morrison, R. W. Hicklin, T. A. Flood Jr, M. F. Richter, and P. J. Hergenrother, Nature chemistry **5**, 195 (2013).
- ⁴² R. Todeschini and V. Consonni, *Handbook of Molecular Descriptors* (Wiley-VCH, Weinheim, 2009).
- ⁴³ J.-L. Faulon, D. P. Visco, Jr., and R. S. Pophale, J. Chem. Inf. Comp. Sci. **43**, 707 (2003).
- ⁴⁴ J. Visco, R. S. Pophale, M. D. Rintoul, and J. L. Faulon, J. Mol. Graph. Model. **20**, 429 (2002).
- ⁴⁵ See Supplemental Material.
- ⁴⁶ N. M. O'Boyle, M. Banck, C. A. James, C. Morley, T. Vandermeersch, and G. R. Hutchison, J. Cheminform. **3**, 1 (2011).
- ⁴⁷ G. Landrum, <http://www.rdkit.org> **3**, 2012 (2014).
- ⁴⁸ F. A. Faber, L. Hutchison, B. Huang, J. Gilmer, S. S. Schoenholz, G. E. Dahl, O. Vinyals, S. Kearnes, P. F. Riley, and O. A. von Lilienfeld, arXiv preprint arXiv:1702.05532 (2017).
- ⁴⁹ K.-R. Müller, S. Mika, G. Rätsch, K. Tsuda, and B. Schölkopf, IEEE transactions on neural networks **12**, 181 (2001).
- ⁵⁰ B. Schölkopf and A. J. Smola, *Learning with kernels: support vector machines, regularization, optimization, and beyond* (MIT press, 2002).
- ⁵¹ V. Vovk, "Kernel ridge regression," in *Empirical Inference: Festschrift in Honor of Vladimir N. Vapnik*, edited by B. Schölkopf, Z. Luo, and V. Vovk (Springer Berlin Heidelberg, Berlin, Heidelberg, 2013) pp. 105–116.
- ⁵² T. Hastie, R. Tibshirani, and J. Friedman, *The Elements of Statistical Learning: Data Mining, Inference, and Prediction, Second Edition*, 2nd ed. (Springer, New York, 2011).
- ⁵³ Hoerl, E. Arthur, Kennard, and W. Robert, Technometrics , 80 (2000).
- ⁵⁴ F. Pedregosa, G. Varoquaux, A. Gramfort, V. Michel, B. Thirion, O. Grisel, M. Blondel, P. Prettenhofer, R. Weiss, V. Dubourg, J. Vanderplas, A. Passos, D. Cournapeau, M. Brucher, M. Perrot, and E. Duchesnay, J. Mach. Learn. Res. **12**, 2825 (2011).
- ⁵⁵ R. M. Neal, *Bayesian Learning for Neural Networks* (Springer-Verlag New York, Inc., Secaucus, NJ, USA, 1996).
- ⁵⁶ H. Zou and T. Hastie, J. R. Stat. Soc. Series. B Stat. Methodol. **67**, 301 (2005).
- ⁵⁷ L. Breiman, Machine learning **45**, 5 (2001).
- ⁵⁸ D. K. Duvenaud, D. Maclaurin, J. Iparraguirre, R. Bombarell, T. Hirzel, A. Aspuru-Guzik, and R. P. Adams, in *Advances in Neural Information Processing Systems*

- (2015) pp. 2215–2223.
- ⁵⁹ T. Desautels, A. Krause, and J. W. Burdick, *J. Mach. Learn. Res.* **15**, 4053 (2014).
- ⁶⁰ “Google hypertune,” <https://cloud.google.com/ml/> (Accessed: 2016).
- ⁶¹ D. P. Tew, W. Klopper, M. Heckert, and J. Gauss, *J. Phys. Chem. A* **111**, 11242 (2007).
- ⁶² K.-R. Müller, M. Finke, N. Murata, K. Schulten, and S. Amari, *Neural Comput.* **8**, 1085 (1996).
- ⁶³ J. Gilmer, S. S. Schoenholz, P. F. Riley, O. Vinyals, and G. E. Dahl, in *Proceedings of the 34th International Conference on Machine Learning, ICML 2017* (2017).
- ⁶⁴ P. Kirkpatrick and C. Ellis, *Nature* **432**, 823 (2004).
- ⁶⁵ S. A. Ghasemi, M. Amsler, R. G. Hennig, S. Roy, S. Goedecker, T. J. Lenosky, C. J. Umrigar, L. Genovese, T. Morishita, and K. Nishio, *Phys. Rev. B* **81**, 214107 (2010).

TABLE III. MAE on out-of-sample data of all representations for all regressors and properties at $\sim 117k$ (90%) training set size. Regressors include Bayesian ridge regression (BR), linear regression with elastic net regularization (EN), random forest (RF), kernel ridge regression (KRR) and molecular graphs based neural networks (GG/GC). The best combination for each property are highlighted in bold. Additionally, the table contains mean absolute deviation (MAD), target MAE, DFT (B3LYP) MAE relative to experiment for all properties in the QM9 data set; mean MAE of representations for each property and regressor; and normalized (by MAD) mean MAE (NMMAE) over all properties for each regressor/representation combination.

		μ	α	$\varepsilon_{\text{HOMO}}$	$\varepsilon_{\text{LUMO}}$	$\Delta\varepsilon$	$\langle R^2 \rangle$	ZPVE	U_0	C_v	ω_1	NMMAE
		Debye	Bohr ³	eV	eV	eV	Bohr ²	eV	eV	cal/molK	cm ⁻¹	arb. u.
Mean		2.67	75.3	-6.54	0.322	6.86	1190	4.06	-76.6	31.6	3500	
MAD		1.17	6.29	0.439	1.05	1.07	203	0.717	8.19	3.21	238	
Target ^a		0.10	0.10	0.043	0.043	0.043	1.2	0.0012	0.043	0.050	10	
DFT ^b		0.10	0.4	2.0	2.6	1.2	-	0.0097	0.10	0.34	28	
EN	CM	0.844	1.33	0.338	0.631	0.722	55.5	0.0265	0.911	0.906	131	0.423
	BOB	0.763	1.20	0.283	0.521	0.614	55.3	0.0232	0.602	0.700	81.4	0.35
	BAML	0.686	0.793	0.186	0.275	0.339	32.6	0.0129	0.212	0.439	60.4	0.231
	ECFP4	0.737	3.45	0.224	0.344	0.383	118	0.270	3.68	1.51	86.6	0.462
	HDAD	0.563	0.437	0.139	0.238	0.278	6.19	0.00647	0.0983	0.0876	94.2	0.183
	HD	0.705	0.638	0.203	0.299	0.360	6.70	0.00949	0.192	0.195	104	0.236
	MARAD	0.707	0.698	0.222	0.305	0.391	27.4	0.00808	0.183	0.206	108	0.256
	Mean	0.715	1.22	0.228	0.373	0.441	43.1	0.0509	0.840	0.578	95.1	
BR	CM	0.844	1.33	0.338	0.632	0.723	55.5	0.0265	0.911	0.907	131	0.424
	BOB	0.761	1.14	0.279	0.521	0.614	48.0	0.0222	0.586	0.684	80.9	0.343
	BAML	0.685	0.785	0.183	0.275	0.339	30.4	0.0129	0.202	0.444	60.4	0.229
	ECFP4	0.737	3.45	0.224	0.344	0.383	118	0.270	3.69	1.51	86.7	0.462
	HDAD	0.565	0.43	0.14	0.238	0.278	5.94	0.00318	0.0614	0.0787	94.8	0.182
	HD	0.705	0.633	0.203	0.298	0.359	6.8	0.00693	0.171	0.19	104	0.235
	MARAD	0.647	0.533	0.18	0.257	0.315	26.8	0.00854	0.171	0.201	103	0.226
	Mean	0.706	1.19	0.221	0.367	0.430	41.7	0.0500	0.828	0.574	94.5	
RF	CM	0.608	1.04	0.208	0.302	0.373	45.0	0.0199	0.431	0.777	13.2	0.239
	BOB	0.450	0.623	0.120	0.137	0.164	39.0	0.0111	0.202	0.443	3.55	0.142
	BAML	0.434	0.638	0.107	0.118	0.141	51.1	0.0132	0.200	0.451	2.71	0.141
	ECFP4	0.483	3.70	0.143	0.145	0.166	109	0.242	3.66	1.57	14.7	0.349
	HDAD	0.454	1.71	0.116	0.136	0.156	48.3	0.0525	1.44	0.895	3.45	0.198
	HD	0.457	1.66	0.126	0.139	0.150	46.8	0.0497	1.39	0.879	4.18	0.197
	MARAD	0.607	0.676	0.178	0.243	0.311	45.3	0.0102	0.21	0.311	19.4	0.199
	Mean	0.499	1.43	0.142	0.174	0.209	54.9	0.0569	1.08	0.761	8.74	
KRR	CM	0.449	0.433	0.133	0.183	0.229	3.39	0.0048	0.128	0.118	33.5	0.136
	BOB	0.423	0.298	0.0948	0.122	0.148	0.978	0.00364	0.0667	0.0917	13.2	0.0981
	BAML	0.460	0.301	0.0946	0.121	0.152	3.9	0.00331	0.0519	0.082	19.9	0.105
	ECFP4	0.490	4.17	0.124	0.133	0.174	128	0.248	4.25	1.84	26.7	0.383
	HDAD	0.334	0.175	0.0662	0.0842	0.107	1.62	0.00191	0.0251	0.0441	23.1	0.0768
	HD	0.364	0.299	0.0874	0.113	0.143	1.72	0.00316	0.0644	0.0844	21.3	0.0935
	MARAD	0.468	0.343	0.103	0.124	0.163	7.58	0.00301	0.0529	0.0758	21.3	0.112
	Mean	0.427	0.859	0.101	0.126	0.159	21.1	0.0383	0.662	0.333	22.7	
GG	MG	0.247	0.161	0.0567	0.0628	0.0877	6.30	0.00431	0.0421	0.0837	6.22	0.0602
GC	MG	0.101	0.232	0.0549	0.0620	0.0869	4.71	0.00966	0.15	0.097	4.76	0.0494

^a Using the same values for target accuracies as in¹³. Target accuracy for energies of atomization, and orbital energies were set to 1 kcal/mol, which is generally accepted as (or close to) chemical accuracy within the chemistry community. Target accuracies used for μ and α are 0.1 D and 0.1 Bohr³ respectively, which is within the error of CCSD relative to experiments²⁹. Target accuracies used for ω_1 and ZPVE are 10⁻¹ cm⁻¹, which is slightly larger than CCSD(T) error for predicting frequencies⁶¹. Target accuracies used for $\langle R^2 \rangle$ and C_v were not explained in article¹³.

^b See section IIC for information on how the errors were obtained.

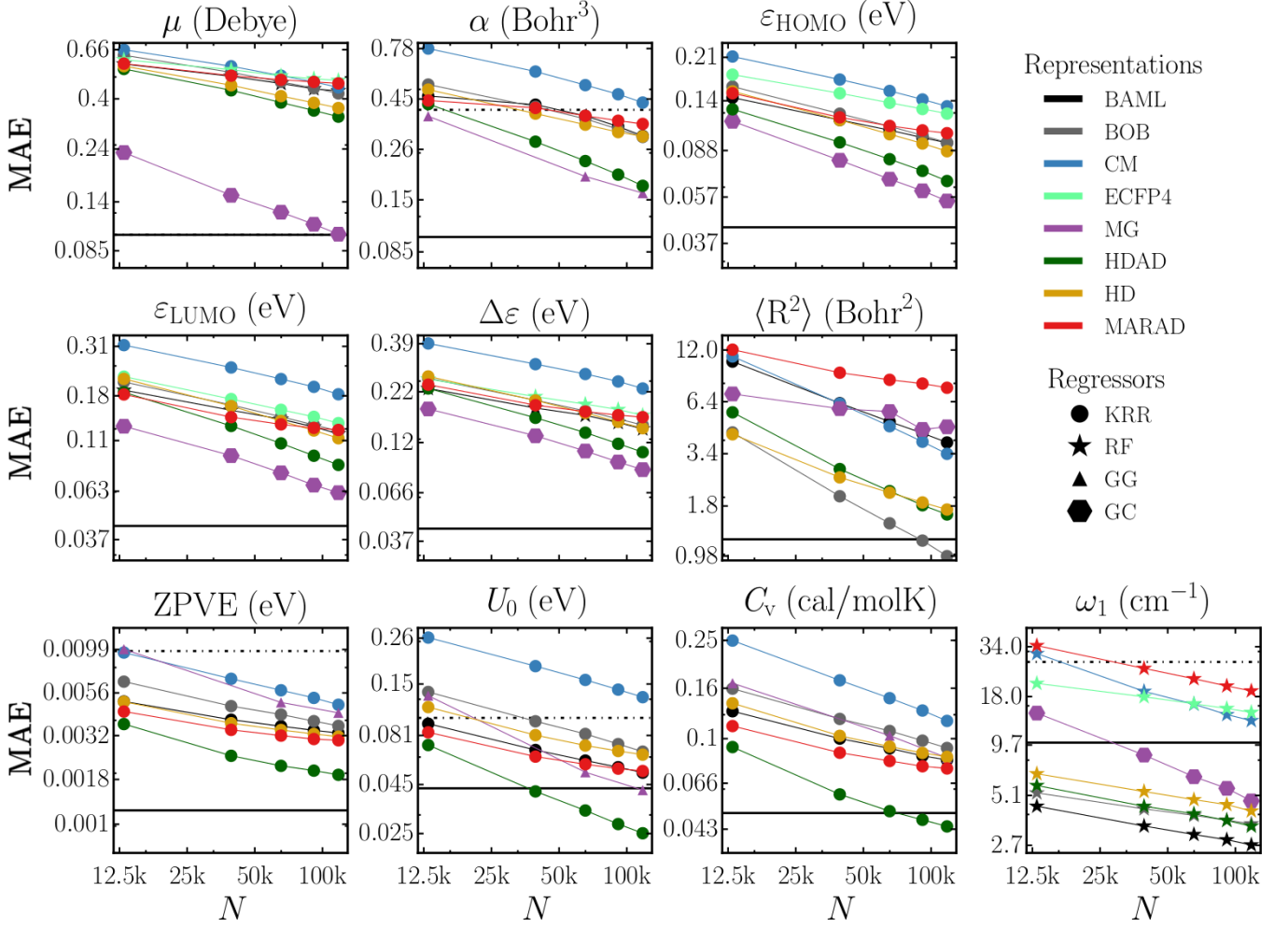


FIG. 2. Learning curves (mean absolute error (MAE) as a function of training set size N) for 10 properties of QM9 molecules, displaying the best regressor for each representation and property. Horizontal solid lines correspond to target accuracies, vertical dotted lines correspond to approximated B3LYP accuracies (unless off-chart), see also table III. Note that due to its poor performance ECFP4 results have been excluded for α , $\langle R^2 \rangle$, ZPVE, U and C_v .